RXTE Observations of the Seyfert 2 Galaxy Mrk 348

David A. Smith[1]

Laboratory for High Energy Astrophysics, NASA/GSFC, Code 662, Greenbelt, MD 20771

Ioannis Georgantopoulos

National Observatory of Athens, Lofos Koufou, Palaia Penteli, 15236 Athens, Greece

and

Robert S. Warwick

Department of Physics and Astronomy, University of Leicester, Leicester LEI 7RH, UK

ABSTRACT

We present RXTE monitoring observations of the Seyfert 2 galaxy Mrk 348 spanning a 6 month period. The time-averaged spectrum in the 3–20 keV band shows many features characteristic of a Compton-thin Seyfert 2 galaxy, namely a hard underlying power-law continuum ($\Gamma \approx 1.8$) with heavy soft X-ray absorption ($N_H \sim 10^{23}$ cm^{-2}) plus measureable iron Kα emission (equivalent width $\sim$ 100 eV) and, at high energy, evidence for a reflection component ($R \lesssim 1$). During the first half of the monitoring period the X-ray continuum flux from Mrk 348 remained relatively steady. However this was followed by a significant brightening of the source (by roughly a factor of 4) with the fastest change corresponding to a doubling of its X-ray flux on a timescale of about 20 days. The flux increase was accompanied by a marked softening of X-ray spectrum most likely attributable to a factor $\sim$ 3 decline in the intrinsic line-of-sight column density. In contrast the iron Kα line and the reflection components showed no evidence of variability. These observations suggest a scenario in which the central X-ray source is surrounded by a patchy distribution of absorbing material located within about a light-week of the nucleus of Mrk 348. The random movement of individual clouds within the absorbing screen, across our line of sight, produces substantial temporal variations in the measured column density on timescales of weeks to months and gives rise to the observed X-ray spectral variability. However, as viewed from the nucleus the global coverage and typical thickness of the cloud layer remains relatively constant.

Subject headings: galaxies: active - galaxies: individual: Markarian 348 - galaxies: Seyfert - X-rays: galaxies

---

[1]also Astronomy Department, University of Maryland, College Park, MD 20742

1. Introduction

The discovery of "hidden" broad-line regions (BLRs) in several Seyfert 2 galaxies (Antonucci & Miller 1985; Miller & Goodrich 1990; Tran et al. 1992) has generated much interest in unified theories, in which the viewing orientation explains many of the observed differences between type 1 and 2 Seyfert galaxies (Antonucci 1993 and references therein). Such theories posit that, in both types of Seyfert galaxy, a luminous central source (presumably an accreting supermassive blackhole) is surrounded by a equatorial distribution of matter in the form of either a swollen accretion disk or a molecular torus (Krolik & Begelman 1986). A type 1 nucleus is then observed only if the viewing direction is sufficiently close to the axis of the system so as to fall within the opening angle of the putative torus. More inclined lines of sight necessarily intercept the disk/torus material in which case we see an "obscured" type 2 system. However, a caveat is that a small fraction of the nuclear flux can be scattered into our line of sight by highly ionized material filling the "hole" of the torus, thus explaining the detection of broad optical lines in polarized light and also weak UV and soft X-ray emission even in Seyfert 2s where our direct view of the nucleus is completely blocked.

X-ray measurements of intrinsic column densities of $\gtrsim 10^{22}$ cm^{-2} in many Seyfert 2 galaxies (Awaki et al. 1991; Smith & Done 1996; Turner et al. 1997a) lend support to the above unification picture. For column densities $\lesssim 10^{24}$ cm^{-2}, X-rays can penetrate the torus leading to the detection of an absorbed power-law continuum together with a iron Kα fluorescence line at 6.4 keV. However for column densities $\gtrsim 10^{24}$ cm^{-2}, even hard X-radiation is seen only indirectly via scattering (as in Compton-thick Seyfert 2s such as NGC 1068). X-rays may be electron scattered by highly ionized matter extending along the axis of the system or Compton reflected by almost neutral material located at the inner edge of the torus. In either case, the scattering material is exposed to the intense nuclear flux and may produce significant line emission and, in circumstances where the direct continuum is completely blocked leaving only a baseline of the much weaker scattered continuum, such lines can have very high equivalent widths (Ghisellini et al. 1994; Krolik et al. 1994).

The spectral indices found in Seyfert galaxies are distributed around a single value of $\Gamma \approx 1.9$ (Nandra & Pounds 1994; Smith & Done 1996). The best explanation for this is that mildly relativistic thermal electrons or highly relativistic non-thermal electrons Compton scatter UV photons into the X-ray energy range (e.g. Svensson 1996 and references therein). The rollover seen in X-ray data above 100 keV has focussed most attention on thermal models (Zdziarski et al. 1995; Gondek et al. 1996). A popular scenario is the two-phase disk-corona model, in which a hot X-ray corona is located above a cold UV emitting accretion disk (Haardt & Maraschi 1991, 1993). The UV seed photons for Compton cooling of the energetic electrons are produced from reprocessing of the hard X-ray spectrum in the accretion disk. With complete feedback, the approximate equipartition between the soft disk and hard X-ray luminosities leads naturally to $\Gamma \gtrsim 1.9$ for a wide range of optical depths (see also Stern et al. 1995). However, for sources with spectra flatter than $\Gamma \approx 1.9$, the disk-corona model of Haardt & Maraschi (1991, 1993) must be modified so that some of the soft seed photons escape without being intercepted by the corona, thus making for harder spectra

as fewer photons are available for Compton scattering (Haardt et al. 1994).

X-ray variability studies of Seyfert 2 nuclei can provide important clues to the processes by which X-rays are produced as well as to the geometry of the circumnuclear matter. However, variability has been reported in only a few objects. One example is Mrk 3, where the hard X-ray emission decreased by a factor of two during a period of 3.6 years (Awaki et al. 1990; Marshall et al. 1992; Iwasawa et al. 1994). Recent observations with *RXTE* have shown variability to exist on time-scales of weeks (Georgantopoulos et al. 1999). The shape of the spectrum suggests that *all* of the variability can be attributed to changes in the direct nuclear flux (Cappi et al. 1999). Short term variability (on time-scales of hours) has been detected in only one object, NGC 4945 (Iwasawa et al. 1993; Guainazzi et al. 2000). These observations suggest that a parsec scale, geometrically thick molecular torus cannot be responsible for the bulk of the X-ray absorption (Madejski et al. 2000).

Spectral variability has also been claimed in a couple of Seyfert 2 galaxies. For example, the absorption column in NGC 7582 increased by $N_{\rm H} \sim 4{\times}10^{22}$ cm^{-2} between *ASCA* observations taken two years apart (Xue et al. 1998). A similar variation in the absorber was suggested by Warwick et al. (1993), based on a comparison between *Einstein*, *EXOSAT*, and *Ginga* observations. More recent observations with *BeppoSAX* of this particular galaxy have shown that the absorber may have a complex spatial structure with a large column density ($N_{\rm H} \sim 10^{24}$ cm^{-2}) covering 60% of hard X-ray continuum, and a smaller, but variable column completely covering the source (Turner et al. 2000). As a further example, in NGC 7172, the spectral index of the power law continuum decreased by $\Delta\Gamma \approx 0.3$ between *Ginga* and *ASCA* observations taken almost 4 years apart (Ryde et al. 1997). These authors attribute the decrease to an intrinsic change in the spectral index although, given the narrow bandpass of *ASCA*, it is possible that the spectrum is affected by a complex absorber and/or Compton reflection.

The launch of the *RXTE* satellite is conducive to the systematic study of variability in Seyfert 2 galaxies, because of the large effective area and broad band coverage afforded by the detectors, and the flexible scheduling allowed by the mission. We have conducted a six month monitoring campaign with *RXTE* of a few Seyfert 2 galaxies previously observed by the *Ginga* and *ASCA* satellites. The results of our observations of Mrk 3 have been reported elsewhere (Georgantopoulos et al. 1999). Here we present our results on Mrk 348.

Mrk 348 is a nearby ($z = 0.015$; de Vaucouleurs et al. 1991) Seyfert 2 galaxy for which there is evidence of a broad (FWHM $\sim$ 7400 km s^{-1}) Hα line component in polarized light (Miller & Goodrich 1990). In terms of current unification schemes for Seyfert galaxies (see above) this can be taken as clear evidence for the presence of an obscured Seyfert 1 nucleus, confirmation of which was provided by the *Ginga* detection of an absorbed ($N_{\rm H} = 10^{23.10\pm0.08}$ cm^{-2}) hard X-ray source (with $\Gamma = 1.68 \pm 0.17$) coincident with this galaxy (Warwick et al. 1989). This heavy obscuration in the nucleus of Mrk 348 may also be responsible for the bi-canonical nature of its ionizing continuum (Mulchaey et al. 1996; Simpson et al. 1996).

There was marginal evidence in the *Ginga* spectrum for an iron Kα emission line at 6.4 keV of equivalent width 130 $\pm$ 130 eV. An iron Kα emission line of equivalent width 113 $\pm$ 56 eV was subsequently detected with *ASCA* (Netzer et al. 1998). In addition to iron Kα, *ASCA* detected a prominent S XIV–XV line of large equivalent width (600 $\pm$ 300 eV). A weak power law continuum was detected at soft X-ray energies in observations made with the *ROSAT* PSPC ($\Gamma = 2.40^{+0.58}_{-0.42}$; Mulchaey et al. 1993) and *ASCA* ($\Gamma = 2.77 \pm 0.87$; Netzer et al. 1998). It is most likely that this weak soft X-ray emission is dominated by electron-scattered nuclear flux, with perhaps some contribution from spatially extended thermal emission from a hot wind (e.g. Krolik & Vrtilek 1984). The 2–10 keV luminosity measured in the *Ginga* observation was 1.2×10^{43} erg s^{-1} ($H_\circ = 50; q_\circ = 0.5$), which is roughly a factor 3 higher than that subsequently recorded by *ASCA*.

2. Observations and Data Analysis

The *Rossi X-ray Timing Explorer (RXTE)* satellite made twelve separate observations of Mrk 348 during the period December 29, 1996 to July 12, 1997, with the intervals between the observations arranged so that the X-ray variability would be sampled on timescales of days, weeks, and months (Table 1). The observation durations were typically in the range 2500–5000 seconds. The instruments on board *RXTE* are the Proportional Counter Array (PCA; Glasser, Odell & Seufert 1994), the High Energy X-ray Timing Experiment (HEXTE; Gruber et al. 1996) and the All-Sky Monitor (ASM; Levine et al. 1996). However, in this paper we consider only the PCA data, since Mrk 348 was not detected by the other instruments. The PCA consists of five sealed proportional counter units (PCUs), with a total collecting area of ~ 6500 cm^2 (Jahoda et al. 1996). The main detector volume of each PCU contains a 90% xenon plus 10% methane gas mixture, and three main layers of anode wires, connected in such a way that two chains of events are produced per layer (Glasser, Odell, & Seufert 1994). The detectors are sensitive to X-rays in the 2–60 keV range, and have an energy resolution equal to $\Delta E/E \sim 18\%$ (FWHM) at 6 keV. The field of view of each PCU is restricted to 1° (FWHM) by a hexagonal, beryllium copper collimator (Jahoda et al. 1996).

Data reduction was carried out using the latest version of the FTOOLS software (version 4.2) together with the standard-2 data files. The standard-2 mode data are the most useful when analysing relatively faint sources, since spectra with full layer identification are accumulated every 16 seconds from "good" xenon events (i.e. those which survive background rejection). For every standard-2 mode data file, a background file is generated using PCABACKEST and the "L7_240" faint source model files. The internal background is correlated with the "L7" rate, which is the sum of the seven two-fold coincidence rates present in the standard-2 mode data files. Most of the internal background can be estimated by matching conditions in the standard-2 files to those in the "L7" model file. However, there is a residual background component associated with activation induced in the spacecraft as it passes through the South Atlantic Anomaly (SAA). In estimating the background due to activation, which has a half-life of 240 minutes, the HEXTE particle monitor

rate is integrated, with an exponential decay term, over the most recent SAA passages. This integrated rate is then multiplied with the activation spectrum in the "240" model file to give the total activation component.

Light curves and spectra were extracted from both the standard-2 mode and background data file, using the standard data selection criteria for faint sources. Only front layer light curves and spectra are considered, as these data have the largest signal-to-noise ratio. The background dominates above 20 keV, so data above this energy are not considered further, and the low energy cut-off for PCA data is 2 keV. PCU3 and PCU4 are occasionally switched off because residue collects on the anodes, so increasing the electric field causing discharge, and therefore the analysis is restricted to data from the first 3 PCUs. Deadtime corrections were not applied, because the correction is very small ($\sim$ 1%) even when the count rate per PCU reaches 1000 count s^{-1}. The individual response matrices for PCU0, PCU1, and PCU2 are co-added prior to spectral fitting.

3. Timing Analysis

The background-subtracted count rates measured in the 2–6 keV band (where the flux is significantly affected by absorption), 6–10 keV band (where the underlying power-law probably dominates the flux), and 10–20 keV band (where Compton reflection may become important) are shown in Figure 1. In all three energy ranges, varability becomes apparent in the second half of the monitoring period and is most evident towards the very end of the campaign. Specifically, the count rate doubles over a period as short as 20 days. The rms variability, after correcting for uncertainties in the background model[2], amounts to 61, 48, and 42% for the 2–6, 6–10 and 10–20 keV bands respectively.

The strong correlation between the signal in the three bands suggests that a single, broad-band spectral component may be responsible for much of the observed variability. The spectral changes implied by the decline in the variability amplitude with energy might result from spectral variations in this component or, alternatively, indicate the presence of two or more spectral components with different temporal behaviour. Further illustration of the X-ray spectral variability is provided by the light curves of the 10–20 keV/6–10 keV and 6–10 keV/2–6 keV hardness ratios, denoted HR1 and HR2 respectively, both of which show a spectral softening as the source intensity increases (see Figure 2).

---

[2]http://lheawww.gsfc.nasa.gov/~dasmith/systematics_000222/systematics_000222.html

4. Spectral Fitting

To improve the signal-to-noise ratio, individual spectra with similar hardness ratio values were combined (i.e., observations 1 & 2; 3 & 4; 5 & 6; 7, 8 & 9; 10 & 11; 12) to give a total of six spectral datasets as input to the spectral fitting analysis, which is based on the XSPEC V10.0 software package (Arnaud 1996).

Above 25 keV, where no signal is expected from Mrk 348 in the front layer, the observed count rates are within 1% of the predicted background count rate. However, below 6 keV, where the mid- and bottom-layer counts rates should be close to the background level, a small deficit is observed in three spectra, which can be removed by decreasing the background by $\leq 5\%$. Hence, the systematic error in the background is considered to be $\leq 5\%$ in three of the six datasets, and $\leq 1\%$ elsewhere. Following Leighly et al. (1999), an estimate of the uncertainties due to the systematic error in the background can be obtained by altering the normalization of the background spectrum by $\pm 1\%$ or $\pm 5\%$. These are shown as additional errors on the spectral parameters.

Fluctuations in the Cosmic X-ray Background (CXB) are also a significant source of uncertainty in the PCA spectra of faint sources. Based on results obtained with the *Ginga* Large Area Counter instrument, the 1σ fluctuation spectrum is best described by a power-law of energy index $\Gamma = 1.8$ and normalization $\pm 2.0 \times 10^{-4}$ photons cm^{-2} sec^{-1} keV^{-1} (Butcher et al. 1997; Reynolds et al. 1999). Hence in our analysis of the X-ray spectrum of Mrk 348, a fluctuation spectrum was included as a separate model component, thus allowing the data themselves to constrain the level of the fluctuation required. This technique was, for example, previously used by Smith & Done (1996) in their analysis of *Ginga* Seyfert 2 spectra.

As a starting point in the spectral analysis all six spectra were fitted by model consisting of a power-law continuum (photon spectral index Γ) absorbed by an intrinsic column density ($N_{\rm H}$), where the atomic cross-sections and abundances for the latter were taken from Bałucińska-Church & McCammon (1992) and Anders & Grevesse (1989), respectively. We also included a narrow ($\sigma_{\rm K\alpha} = 0.1$ keV) Gaussian emission line to represent the iron Kα emission. Initially, only the power-law normalization was allowed to vary across the six spectra with the line energy fixed at 6.4 keV, the value for neutral iron. This model (model 1) provides an unacceptable fit with $\chi^2 = 484.2$ for $= 302$ degrees of freedom (d.o.f.), the best-fitting parameters being $\Gamma = 1.54^{+0.03}_{-0.04}$ and $N_{\rm H} = 10.1^{+0.5}_{-0.6} \times 10^{22}$ cm^{-2} (the errors, here and elsewhere in this paper, are 90% confidence for one interesting parameter, $\Delta\chi^2 = 2.7$). Given the spectral variability evident in the data (see section 3), it is not surprising that this model rather poorly describes the observed spectra.

The next step was to allow either the column density (model 2) or the photon index (model 3) to vary across the six spectra. The variable column density description provides an excellent fit, with $\Gamma = 1.58 \pm 0.03$ and $N_{\rm H}$ in the range ($8.6^{+0.8}_{-0.6}$ to $31.8^{+5.5}_{-4.6}$) $\times 10^{22}$ cm^{-2} ($\chi^2 = 202.1$, 297 d.o.f.). Consistent with the observed hardness ratio variations, the column density falls as the power-law normalization (and hence the intrinsic flux) increases. The variable index model provides a worse fit, but nevertheless one which is still excellent, with Γ in the range $0.92^{+0.09}_{-0.10}$ to

$1.68^{+0.05}_{-0.04}$ and $N_{\rm H} = 9.8^{+0.5}_{-0.5} \times 10^{22}$ cm^{-2} ($\chi^2 = 221.5$, 297 d.o.f.). In this case there is a strong correlation between photon index and intrinsic flux, with a steeper spectral index being preferred in the brighter source states (see Table 2 for details of both model 2 and model 3 spectral fitting results). The 2–10 keV luminosity measured in the *RXTE* observations was (0.8–3.4) $\times 10^{43}$ ergs s^{-1} ($H_\circ = 50; q_\circ = 0.5$), which implies a peak intensity a factor 3 higher than that recorded by *Ginga*.

In the variable column density description (model 2), the *unabsorbed* iron Kα emission line flux was $2.1^{+0.8}_{-0.7} \times 10^{-5}$ photon s^{-1} cm^{-2}, yielding an equivalent width, with respect to the *absorbed* continuum, in the range 40–170 eV. This is consistent with the emission line fluxes determined from earlier *Ginga* ($5.0 \pm 2.2 \times 10^{-5}$ photon s^{-1} cm^{-2}; Smith & Done 1996) and *ASCA* ($1.4 \pm 0.7 \times 10^{-5}$ photon s^{-1} cm^{-2}; Netzer, Turner & George 1998) observations, although the uncertainties in the individual measurements are rather large. Assuming a spherical distribution of gas, the equivalent width expected from the measured column density would be in the range 40–130 eV (Leahy & Creighton 1993), comparable to that observed. We note that the best-fit line energy is 6.15 ± 0.14 keV, which is below that expected for cold iron. However, we suspect this discrepancy is due to uncertainties in the instrument response around the Xe L edge at ~ 5 keV. Finally, if the line normalization is allowed to vary between the six spectra, the reduction in χ^2 is ~ 3, which is not statistically significant (on the basis of the F-test for five additional free parameters; Bevington & Robinson 1992). Although this lack of line variability is intriguing, the rather large uncertainties in the individual measurements and coarse sampling do not exclude the possibility that the line flux tracks the continuum on timescales as short as hours, as would be expected if most of the line was produced in a putative accretion disk.

While the spectra fits confirm the presence of spectral variability, the origin of the changes in either column density and/or photon index variations is not distinguishable. Therefore, as an additional test, the data were separated into two spectra on the basis of the flux change that occurred during the latter part of the monitoring campaign. Thus, data from the first six observations were combined into a "low state" spectrum, while data from the last six spectra comprise a "high state" spectrum. These two spectra were then fitted to a spectral model in which *both* the column density and photon index were allowed to vary. The projected confidence regions in the Γ–$N_{\rm H}$ plane for this model are shown in Figure 3. Although photon index variations cannot be excluded, a significant change in the column density is required by the data. Hereafter we take the view that, on the basis of these very simple spectral models, the spectral variability is best assigned largely to variations in the column density.

Although the above absorbed power-law model provides an excellent fit to the combined *RXTE* datasets, we next consider what constraints, if any, may be placed on slightly more sophisticated spectral descriptions, such as models including either a Compton reflection component or a partially covered source. Specifically we considered the possibility that some of the observed spectral variability may arise due to the presence of an extra component with a delayed temporal response relative to the direct continuum.

If the disk-corona model described in §1 is correct, then a significant fraction of the hard X-ray flux should be reprocessed in the accretion disk. The anticipated spectral signatures from such reprocessing includes an iron Kα fluorescence line and Compton reflection of the hard continuum (George & Fabian 1991; Matt et al. 1991). These features have previously been identified in many Seyfert galaxies, and may also be present in the spectrum of Mrk 348. Motivated by this prediction, the data were fitted to a model consisting of an absorbed power-law continuum with *absorbed* Compton reflection from neutral, solar abundant material, as implemented in the PEXRAV model (Magdziarz & Zdziarski 1995) plus a narrow Gaussian line representing iron Kα emission (model 4). The inclination (to our line of sight) of the reflecting material was fixed at the default value ($i = 60°$), since the reflection spectrum below 20 keV is relatively independent of the inclination angle. The shape of the incident continuum above 20 keV is important, even when considering measurements below this energy because of the effects of Compton down-scattering; the power-law continuum was therefore exponentially cut-off with an e-folding energy of 150 keV, similar to that observed in other Seyfert galaxies (Zdziarski et al. 1995; Gondek et al. 1996).

The reflected spectrum should track the continuum on timescales of weeks or less, if it originates in the putative disk. Therefore, the relative normalization between the direct and reflected continuum was initially tied to a single value for all six spectra (a value of $\mathcal{R} = 1$ is expected from a flat $\Omega/2\pi = 1$ geometry and isotropic emission). In this case the best-fitting parameter values are $\Gamma = 1.67^{+0.03}_{-0.04}$, $\mathcal{R} = 0.5^{+0.2}_{-0.3}$ and $N_{\rm H}$ in the range $(9.1 \pm 0.6$ to $27.5^{+4.9}_{-5.4}) \times 10^{22}$ cm^{-2} ($\chi^2 = 193.4$; $d.o.f. = 296$; see Table 3). This model provides a significantly ($> 99\%$) better fit to the data (on the basis of a F-test for one additional free parameter), than our earlier preferred model (model 2). The iron Kα emission line flux was $1.7^{+0.8}_{-0.7} \times 10^{-5}$ photons s^{-1} cm^{-2}, which yields an equivalent width in the range 40–120 eV, compared with the $\sim$ 50 eV equivalent width expected from the reflection continuum (George & Fabian 1991; Matt et al. 1991; Ghisellini et al. 1994). Thus, for the brighter source states, reflection could produce all of the observed line emission. When the relative strength of the reflection continuum is allowed to vary between the observations, there is a strong correlation between its strength and the intensity of the source, with a stronger reflection continuum being preferred for the weaker source states. However, the reduction in χ^2 of $\Delta\chi^2 \approx 5$ is insignificant (on the basis of a F-test for six additional free parameters) and, therefore, we cannot draw any firm conclusions.

If the molecular torus is optically thick, then Compton reflection originating at the (far-side) inner walls of the torus may be seen directly, rather than through the gas column responsible for the low energy absorption (depending, of course, on the torus geometry and view angle). Such reflection would not be expected to vary on timescales shorter than about a year, and could in principle lead to a net softening of the spectrum as the source intensity increases. Such reflection could also contribute significantly to a non-varying component of the iron Kα emission line. To test this possibility, the data were fitted to a model including an absorbed power-law continuum, an *unabsorbed and non-variable* Compton reflection component, and a narrow Gaussian emission line (model 5). The Compton reflection spectrum was the same as that used for model 4. The best-fit

values are $\Gamma = 1.65 \pm 0.05$ and $N_{\rm H}$ in the range ($9.8^{+0.9}_{-0.7}$ to $32.4^{+6.8}_{-6.2}$) $\times 10^{22}$ cm^{-2} ($\chi^2 = 188.5$; $d.o.f = 296$; see Table 3). The improvement in χ^2 over that for the variable absorber model is significant at $> 99\%$ (on the basis of a F-test for one additional term). The relative normalization between the direct and reflected continua varies from $\mathcal{R} \approx 0.3$ to $\mathcal{R} \approx 0.8$ as the level of the former changes. The iron Kα emission line flux was $1.6 \pm 0.7 \times 10^{-5}$ photons s^{-1} cm^{-2}, and yields an equivalent width in the range 30–120 eV, comparable to the 30-100 eV range expected from reflection continuum alone.

Recently, evidence has emerged for Compton-thick material which partially, or fully covers the central nucleus in several Seyfert 2 galaxies (NGC 4945, Iwasawa et al. 1993, Done, Madejski & Smith 1996; IRAS 04575-7537, Vignali et al. 1998; Mrk 3, Turner et al. 1997b, Cappi et al. 1999, Georgantopoulos et al. 1999; NGC 7582, Turner et al. 2000). In order to test for the presence of Compton-thick material obscuring the nucleus in Mrk 348, the data were fitted to a model consisting of a power-law continuum, which is partially covered by a constant column ($N_{\rm H1}$), and fully covered by a variable absorber ($N_{\rm H2}$), plus a narrow Gaussian emission line (model 6). This model provides the best fit so far to the data, with $\Gamma = 1.77^{+0.10}_{-0.05}$, $N_{\rm H1} = (111^{+52}_{-32}) \times 10^{22}$ cm^{-2} covering $0.24^{+0.03}_{-0.07}$ of the source, and $N_{\rm H2}$ in the range ($9.7^{+0.8}_{-0.6}$ to $31.9^{+5.3}_{-5.1}$) $\times 10^{22}$ cm^{-2} ($\chi^2 = 184.9$; $d.o.f. = 295$; see Table 4). The iron Kα line equivalent width expected from an obscuring column of $N_{\rm H} \sim 10^{24}$ cm^{-2} would be ~ 500 eV (Leahy & Creighton 1993) with respect to the absorbed continuum, but only ~ 100 eV with respect to the unabsorbed continuum, and so would remain largely undetected in these data, given the small covering fraction. We note also, that the best-fit photon index is $\Gamma \sim 1.8$, which is close to that found in other Seyfert nuclei (Nandra & Pounds 1994; Smith & Done 1996).

5. Discussion

The shortest timescale on which X-ray continuum variations are observed in Mrk 348 is $\sim$ 1 day, the minimum spacing between observations. In terms of the light-travel time this implies a maximum source size of $r_{\rm s} \simeq 2.5 \times 10^{15}$ cm, although in reality the X-ray emitting region may be much smaller than this, (i.e. $\sim 3 \times 10^{14}$ cm if the X-rays are produced within 10 Schwarzchild radii of a 10^8 $M_\odot$ black hole). In contrast variations in the intrinsic column density (along the line of sight to the nucleus of Mrk 348) take place over periods of typically weeks to months with the largest change, $\Delta N_{\rm H} \sim 10^{23}$ cm^{-2}, occurring on a timescale of ~ 70 days.

If the observed column changes are interpreted as due to the motion, across the line of sight, of clouds of gaseous material in orbit around the central black-hole, then for a transverse cloud velocity of $v_{\rm cloud} \approx 10,000$ km s^{-1} (characteristic of extreme BLR cloud velocities), the predicted timescale for the column change is $r_{\rm s}/v_{\rm cloud} \simeq 30$ days, which is roughly consistent with the observations. Such clouds are located at a distance of $R = GM/v^2_{\rm cloud} \simeq 1.3 \times 10^{16} M_8$ cm, where M_8 is the black-hole mass in units of 10^8 $M_\odot$. We can infer the ionization of the cloud material via the ionization parameter ξ, where $\xi = L_{\rm ion}/n_{\rm e}R^2$. Here $L_{\rm ion}$ is the ionizing luminosity (measured

between 13.6 eV to 13.6 keV; Kallman & McCray 1982), n_e is the gas density and R is the distance to the clouds from the continuum source. For an ionizing luminosity of $\sim 5 \times 10^{43}$ erg s^{-1} and $n_e \approx 10^{10}$ cm^{-3} (a typical value for BLR clouds), the ionization parameter is $\xi \approx 30$. This is consistent with a lightly ionized state for the iron in the clouds (i.e. below FeXV), but in agreement with the iron Kα emission-line (and K-edge) requirements. However for a typical cloud column density of $\Delta N_H \sim 10^{23}$ cm^{-2}, the implied physical thickness, is only $\Delta N_H / n_e \sim 10^{13}$ cm. Since this dimension is much smaller than the inferred X-ray source size r_s, the organisation of clouds into a coherent sheet-like distribution is required in order to explain the large amplitude N_H variations which are observed in Mrk 348 and other sources (e.g. Yaqoob et al. 1993).

Alternatively, the increase in the source luminosity may be sufficient to induce the observed decline in the column density via photo-ionization. However, the lack of evidence for highly ionized iron in Mrk 348 would require a fairly narrow regime for the ionization parameter. Such a scenario could be investigated using photo-ionization codes such as XSTAR, but this is beyond the scope of the present paper.

Within the measurement constraints, the iron Kα line flux remained at a roughly constant level throughout the monitoring campaign. This implies that much of the line emission is produced in material reasonably distant from the nucleus. A possible location for this material is in the patchy cloud distribution responsible for the highly variable intrinsic absorption in this source. The lack of significant changes in the line flux then requires both the sky coverage and typical thickness of the cloud layer, as viewed from the nucleus, to remain fairly constant (a requirement which need not, of course, conflict with the fact that temporal variations are observed along our specific line of sight). It is also possible that a contribution to the line emission comes from the illumination of the (far-side) inner walls of the putative molecular torus (assuming at least some element of the gaseous medium surrounding the X-ray source is Thomson thick). While Compton reflection is not specifically required by the spectral fitting, the data are consistent with the reflection expected from a torus subtending a solid angle at the source of $\Omega/2\pi \approx 0.3$–0.8. If the ionization cones are collimated by the torus, then the observed half-opening angle of the cones, of $\theta \sim 45°$ (Simpson et al. 1996), corresponds to a torus solid angle of order $\Omega/2\pi = 2\cos\theta = 1.4$. Thus, in principle the bulk of the line emission could originate in this way. In this setting, the fact that Mrk 348 is not observed as a Compton-thick Seyfert 2 is presumably the result of our line of sight to the nucleus passing across the top of the torus thus avoiding its most optically thick regions.

Finally, we note that the iron Kα emission observed in the X-ray spectra of many Seyfert 1 galaxies is most naturally associated with reflection from the inner regions of an accretion disk. One signature of such emission is the broadening of the line due to relativistic effects close to the central massive black-hole (e.g. Tanaka et al. 1995). Also, depending on the geometry and optical depth of the X-ray emitting plasma, variations in the line flux on timescales of a week or less are predicted. The current observations provide no evidence for such an origin for the iron Kα emission observed in Mrk 348. Also an earlier *ASCA* observation of Mrk 348 was unable to determine whether the iron Kα emission line was significantly broadened (Netzer et al. 1998). Clearly further observations with

much higher signal-to-noise and energy resolution will be needed in order to test for the presence of an accretion disk in Mrk 348.

REFERENCES

Anders, E., & Grevesse, N. 1989, Geochimica et Cosmochimica Acta, 53, 197

Antonucci, R. R. J., & Miller, J. S. 1985, ApJ, 297, 621

Antonucci, R. 1993, ARA&A, 31, 473

Arnaud, K. A. 1996, in ASP Conf. Proc. 101, Astronomical Data Analysis Software and Systems V, ed. G. Jacoby & J. Barnes (San Francisco: ASP), 17

Awaki, H., Koyama, K., Kunieda, H., & Tawara, Y. 1990, Nature, 346, 544

Awaki, H., Koyama, K., Inoue, H., & Halpern, J. P. 1991, PASJ, 43, 195

Bałucińska-Church, M., & McCammon, D. 1992, ApJ, 400, 699

Bevington, P. R., & Robinson, D. K. 1992, Data Reduction and Error Analysis for the Physical Sciences, McGraw-Hill, New York

Butcher, J. A., Stewart, G. C., Warwick, R. S., Fabian, A. C., Carrera, F. J., Barcons, X., Hayashida, K., Inoue, H., Kii, T. 1997, MNRAS, 291, 437

Cappi, M., Bassani, L., Comastri, A., et al. 1999, A&A, 344, 857

de Vaucouleurs, G., de Vaucouleurs, A., Corwin, H., Buta, R. J., Paturel, G., & Fouqu, P. 1991, Third Reference Catalogue of Bright Galaxies (Berlin: Springer)

Done, C., Madejski, G. M., & Smith, D. A. 1996, ApJ, 463, L63

Georgantopoulos, I., Papadakis, I., Warwick, R. S., Smith, D. A., Stewart, G. C., & Griffiths, R. G. 1999, MNRAS, 307, 815

George, I. M., & Fabian, A. C. 1991, MNRAS, 249, 352

Ghisellini, G, Haardt, F., Matt, G. 1994, MNRAS, 267, 743

Glasser, C. A., Odell, C. E., & Seufert, S. E. 1994, IEEE Trans. Nucl. Sci., 41, 1343

Gondek, D., Zdziarski, A. A., Johnson, W. N., George, I. M., McNaron-Brown, K., Magdziarz, P., Smith, D., & Gruber, D. E. 1996, MNRAS, 282, 646

Gruber, D. E., Blanco, P. R., Heindl, W. A., Pelling, M. R., Rothschild, R. E., & Hink, P. L. 1996. A&ASS, 120, 641

Guainazzi, M., Matt, G., Brandt, W. N., Antonelli, L. A., Barr, P., & Bassani, L. 2000, A&A, accepted

Haardt, F., & Maraschi, L. 1991, ApJ, 380, L51

Haardt, F., & Maraschi, L. 1993, ApJ, 413, 680

Haardt, F., Maraschi, L., & Ghisellini, G. 1994, ApJ, 432, L95

Iwasawa, K., Koyama, K., Awaki, H., Kunieda, H., Makishima, K., Tsuru, T., Ohashi, T., & Nakai, N. 1993, ApJ, 409, 155

Iwasawa, K., Yaqoob, T., Awaki, H., & Ogasaka, Y. 1994, PASJ, 46, L167

Jahoda, K., Swank, J. H., Giles, A. B., Stark, M. J., Strohmayer, T., Zhang, W., & Morgan, E. 1996, SPIE, 2808, 59

Kallman, T. R., & McCray, R. 1982, ApJS, 50, 263

Krolik, J. H., & Vrtilek, J. M. 1984, ApJ, 279, 521

Krolik, J. H., & Begelman, M. C. 1986, ApJ, 308, L55

Krolik, J. H., Madau, P., & Życki, P. T. 1994, ApJ, 420, L57

Leahy, D. A., & Creighton, J. 1993, MNRAS, 263, 314

Levine, A. M., Bradt, H., Cui, W., Jernigan, J. G., Morgan, E. H., Remillard, R., Shirey, R. E., & Smith, D. A. 1996, ApJ, 469, L33

Leighly, K. M., Halpern, J. P., Awaki, H., Cappi, M., Ueno, S., & Siebert, J. 1999, ApJ, 522, 209

Madejski, G. M., Życki, P. T., Done, C., Valinia, A., Blanco, P., Rothschild, R., Turek, B. 2000, ApJ, accepted

Magdziarz, P. & Zdziarski, A. A. 1995, MNRAS, 273, 837

Marshall, F. E., Boldt, E. A., Holt, S. S., et al. 1992, in Frontiers of X-ray Astronomy, ed. Tanaka, Y. & Koyama, K. (Tokyo: Universal Academy Press), 233

Matt, G., Perola, G. C., & Piro, L. 1991, A&A, 247, 25

Miller, J. S. & Goodrich, R. W. 1990, ApJ, 355, 456

Mulchaey, J. S., Colbert, E., Wilson, A. S., Mushotzky, R. F., & Weaver, K. A. 1993, ApJ, 414, 144

Mulchaey, J. S., Wilson, A. S., & Tsvetanov, Z. 1996, ApJS, 102, 309

Nandra, K., & Pounds, K. A. 1994, MNRAS, 268, 405

Netzer, H., Turner, T. J., & George, I. M. 1998, ApJ, 504, 680

Reynolds, C. S., Heinz, S., Fabian, A.,C., & Begelman, M. C. 1999, ApJ, 521, 99

Ryde, F., Poutanen, J., Svensson, R., Larsson, S., & Ueno, S. 1997, A&A, 328, 69

Simpson, C., Mulchaey, J. S., Wilson, A. S., Ward, M. J., & Alonso-Herrero, A. 1996, ApJ, 457, L19

Smith, D. A. & Done, C. 1996, MNRAS, 280, 355

Svensson, R. 1996, A&AS, 120, 475

Tanaka, Y., Nandra, K., Fabian, A. C., et al. 1995, Nature, 375, 659

Tran, H. D., Miller, J. S., & Kay, L. E. 1992, ApJ, 397, 452

Turner, T. J., George, I. M., Nandra, K., & Mushotzky, R. F. 1997a, ApJS, 113, 23

Turner, T. J., George, I. M., Nandra, K., & Mushotzky, R. F. 1997b, ApJ, 488, 164

Turner, T. J., Perola, G. C., Fiore, F., Matt, G., George, I. M., Piro, L., Bassani, L. 2000, ApJ, 531, 245

Vignali, C., Comastri, A., Stirpe, G. M., Cappi, M., Palumbo, G. G. C., Matsuoka, M., Malaguti, G., & Bassani, L. 1998, A&A, 333, 411

Warwick, R. S., Koyama, K., Inoue, H., Takano, S., Awaki, H., & Hoshi, R. 1989, PASJ, 41, 739

Warwick, R. S., Sembay, S., Yaqoob, T., Makishima, K., Ohashi, T., Tashiro, M., & Kohmura, Y. 1993, MNRAS, 265, 412

Xue, S.-J., Otani, C., Mihara, T., Cappi, M., & Matsuoka, M. 1998, PASJ, 50, 519

Yaqoob, T., Warwick, R. S., Makino, F., Otani, C., Sokoloski, J. L., Bond, I. A., & Yamauchi, M. 1993, MNRAS, 262, 435

Zdziarski, A. A., Johnson, W. N., Done, C., Smith, D., & McNaron-Brown, K. 1995, ApJ, 438, L63

Fig. 1.— Background-subtracted X-ray light curves in the 2-6, 6-10, and 10-20 keV bands.

Fig. 2.— Light curves of the 10–20 keV/6–10 keV and 6–10 keV/2-6 keV hardness ratios, denoted HR1 and HR2 respectively.

Fig. 3.— The projected confidence regions in the Γ–$N_{\rm H}$ plane for the high (leftmost contour) and low state (rightmost contour) data. The contours are $\Delta\chi^2 = 2.30$, 4.61, and 9.21 (i.e. 68, 90, and 99% confidence for two interesting parameters).

Table 1. Observations.

ObsId[a]	Start time[b]	Stop time[b]	Exposure[c]	Count rate[d]
20330-02-01-00	1996-12-29 09:36:10	1996-12-29 11:34:13	4656	2.56 ± 0.05
20330-02-02-00	1997-02-07 04:28:07	1997-02-07 07:08:14	3744	2.23 ± 0.06
20330-02-03-00	1997-03-04 05:42:23	1997-03-04 07:48:13	4112	2.01 ± 0.06
20330-02-04-00	1997-03-21 22:24:36	1997-03-22 01:14:13	4064	2.03 ± 0.06
20330-02-05-00	1997-05-08 21:45:36	1997-05-09 00:05:13	2640	4.00 ± 0.08
20330-02-06-00	1997-05-30 00:20:35	1997-05-30 02:20:13	3216	4.77 ± 0.07
20330-02-07-00	1997-06-27 20:30:56	1997-06-27 23:25:13	2464	6.50 ± 0.08
20330-02-08-00	1997-06-28 20:17:10	1997-06-28 23:29:13	3616	7.15 ± 0.07
20330-02-09-00	1997-06-29 23:19:33	1997-06-30 01:36:13	3792	9.06 ± 0.07
20330-02-10-00	1997-07-03 21:40:20	1997-07-04 00:01:14	4384	8.28 ± 0.07
20330-02-11-00	1997-07-04 20:01:16	1997-07-04 22:04:14	3568	10.60 ± 0.08
20330-02-12-00	1997-07-12 00:06:59	1997-07-12 03:21:14	3760	10.61 ± 0.08

[a]Observational Identification

[b]Coordinated Universal Time

[c]Approximate exposure time (seconds)

[d]Count s^{-1}, 2-10 keV

Table 2. Absorbed power-law plus line fits.

	Model 2				Model 3			
Dataset	A^a	Γ^b	$N_H{}^c$	$F_X{}^d$	A^a	Γ^b	$N_H{}^c$	$F_X{}^d$
1	4.0	$1.58^{+0.03-0.10}_{-0.03+0.09}$	$22.7^{+4.1-1.3}_{-3.4-1.5}$	0.8	1.3	$1.15^{+0.09-0.08}_{-0.09+0.07}$	$9.8^{+0.5-1.4}_{-0.5+1.2}$	0.8
2	4.3	···	$31.8^{+5.5-2.8}_{-4.6-1.5}$	0.7	0.7	$0.92^{+0.10-0.12}_{-0.10+0.12}$	···	0.7
3	6.2	···	$15.7^{+2.0-1.8}_{-1.5-0.5}$	1.5	3.5	$1.35^{+0.06-0.12}_{-0.06+0.12}$	···	1.5
4	9.3	···	$10.4^{+0.9-1.2}_{-0.6-0.6}$	2.6	9.1	$1.57^{+0.04-0.08}_{-0.04+0.07}$	···	2.5
5	9.9	···	$11.3^{+1.0-1.4}_{-0.6-0.8}$	2.7	8.6	$1.52^{+0.04-0.11}_{-0.04+0.11}$	···	2.6
6	11.8	···	$8.6^{+0.8-1.2}_{-0.6-0.7}$	3.5	15.1	$1.68^{+0.05-0.08}_{-0.05+0.08}$	···	3.5

[a]Flux of the unabsorbed power-law continuum at 1 keV in units of 10^{-3} photons cm^{-2} sec^{-1}

[b]Photon spectral index

[c]Measured column expressed in units of 10^{22} cm^{-2}

[d]Flux expressed in units of 10^{-11} erg cm^{-2} s^{-1}

Note. — Two kinds of errors are given here, and in subsequent tables. The first one is the statistical error (see text). The second one is an estimate of the uncertainty due to the systematic error in the background subtraction. The results from decreasing and increasing the background are given by the superscript and subscript values respectively.

Table 3. Spectral fits with the Compton reflection spectrum.

	Model 4				Model 5			
Dataset	A^a	Γ^b	$N_H{}^c$	$F_X{}^d$	A^a	Γ^b	$N_H{}^c$	$F_X{}^d$
1	4.2	$1.67^{+0.03-0.03}_{-0.03+0.06}$	$19.9^{+3.0-2.3}_{-3.7-0.4}$	0.8	4.1	$1.65^{+0.05-0.01}_{-0.05+0.05}$	$23.0^{+4.9-2.2}_{-4.2-2.9}$	0.7
2	4.4	···	$27.5^{+4.9-2.0}_{-5.4-1.8}$	0.6	4.3	···	$32.4^{+6.8-2.3}_{-6.1-3.6}$	0.6
3	7.0	···	$15.1^{+1.6-0.4}_{-1.9-0.8}$	1.5	6.7	···	$16.8^{+2.3-1.1}_{-2.0-2.4}$	1.4
4	10.1	···	$10.7^{+0.6-0.2}_{-1.0-0.4}$	2.7	10.3	···	$11.6^{+0.9-1.0}_{-1.0-1.3}$	2.6
5	11.6	···	$11.6^{+0.7-0.1}_{-1.0-0.5}$	2.8	11.1	···	$12.7^{+1.0-1.0}_{-1.1-1.4}$	2.6
6	14.0	···	$9.1^{+0.6-0.1}_{-0.6-0.4}$	3.8	13.3	···	$9.8^{+0.9-0.8}_{-0.7-0.9}$	3.6

[a]Flux of the unabsorbed power-law continuum at 1 keV in units of 10^{-3} photons cm^{-2} sec^{-1}

[b]Photon spectral index

[c]Measured column expressed in units of 10^{22} cm^{-2}

[d]Flux expressed in units of 10^{-11} erg cm^{-2} s^{-1}

Table 4. Partial coverer fit.

	Model 6					
Dataset	A[a]	Γ[b]	N_{H1}[c]	C_F[d]	N_{H2}[c]	F_X[e]
1	7.7	$1.77^{+0.10-0.07}_{-0.05+0.07}$	$111^{+52+113}_{-32-54}$	$0.24^{+0.03+0.11}_{-0.07-0.01}$	$23.4^{+4.0+0.0}_{-3.6-2.0}$	0.8
2	8.0	...	...	...	$31.9^{+5.4-1.1}_{-5.1-1.6}$	0.6
3	11.8	...	...	...	$16.8^{+2.0-0.7}_{-1.9-0.3}$	1.5
4	17.5	...	...	...	$11.5^{+0.9-0.4}_{-0.7-0.2}$	2.7
5	18.8	...	...	...	$12.5^{+1.1-0.5}_{-0.7-0.1}$	2.8
6	22.3	...	...	...	$9.7^{+0.8-0.5}_{-0.6-0.1}$	3.8

[a]Flux of the unabsorbed power-law continuum at 1 keV in units of 10^{-3} photons cm^{-2} sec^{-1}

[b]Photon spectral index

[c]Measured column expressed in units of 10^{22} cm^{-2}

[d]Covered fraction

[e]Flux expressed in units of 10^{-11} erg cm^{-2} s^{-1}

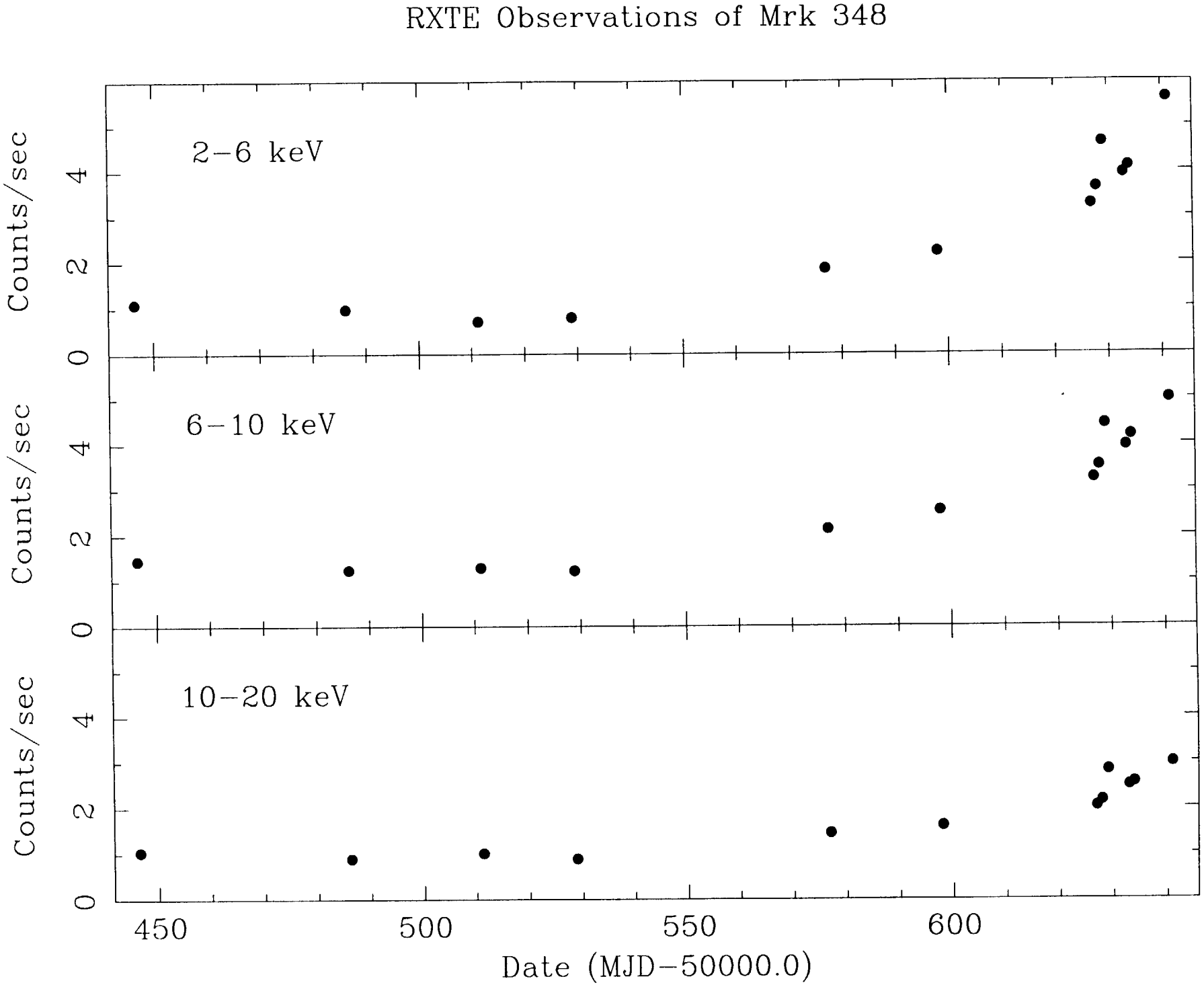
RXTE Observations of Mrk 348
2–6 keV
6–10 keV
10–20 keV
Counts/sec
0
2
4
450
500
550
600
Date (MJD−50000.0)

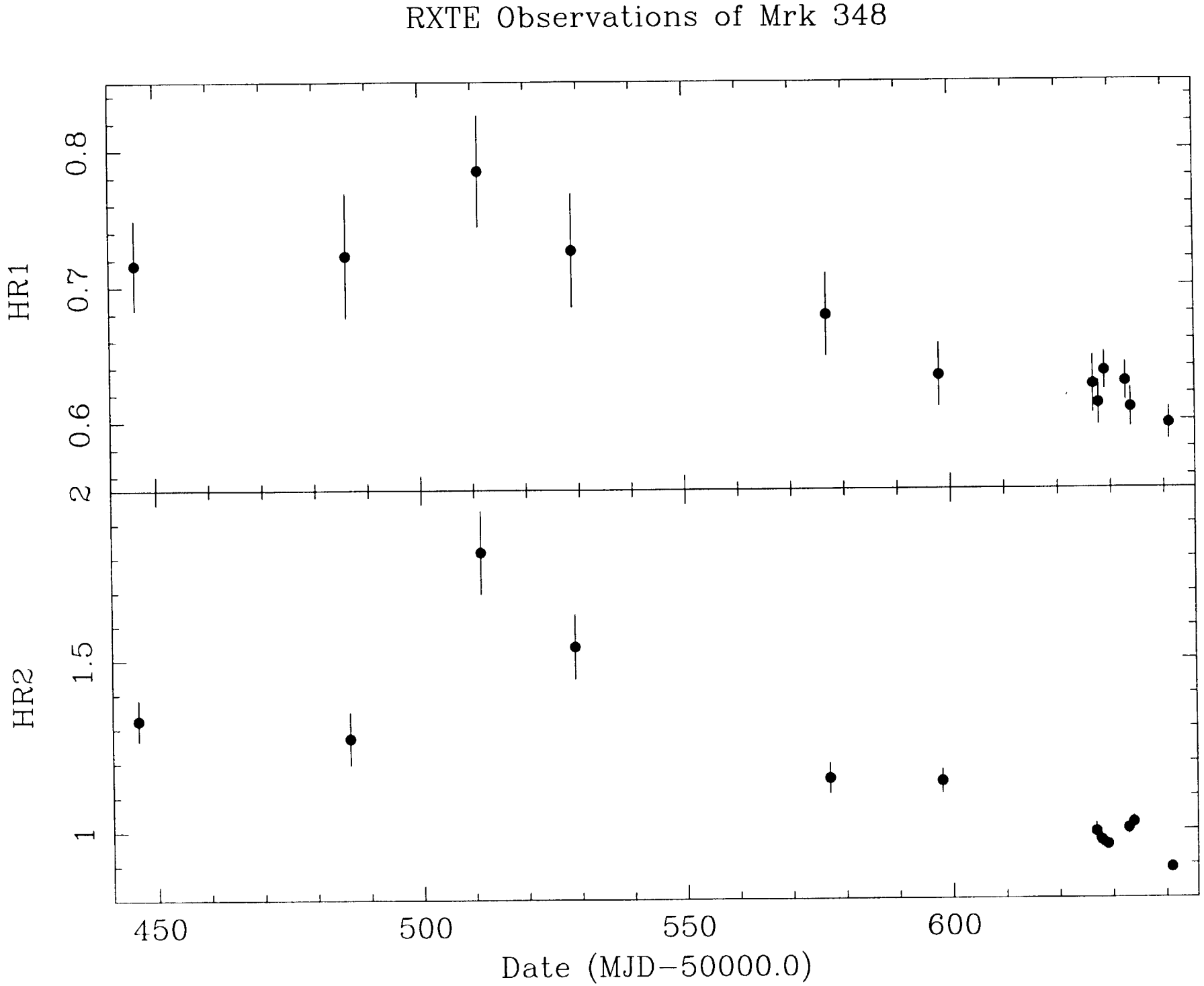
RXTE Observations of Mrk 348
HR1
0.8
0.7
0.6
2
HR2
1.5
1
450
500
550
600
Date (MJD−50000.0)

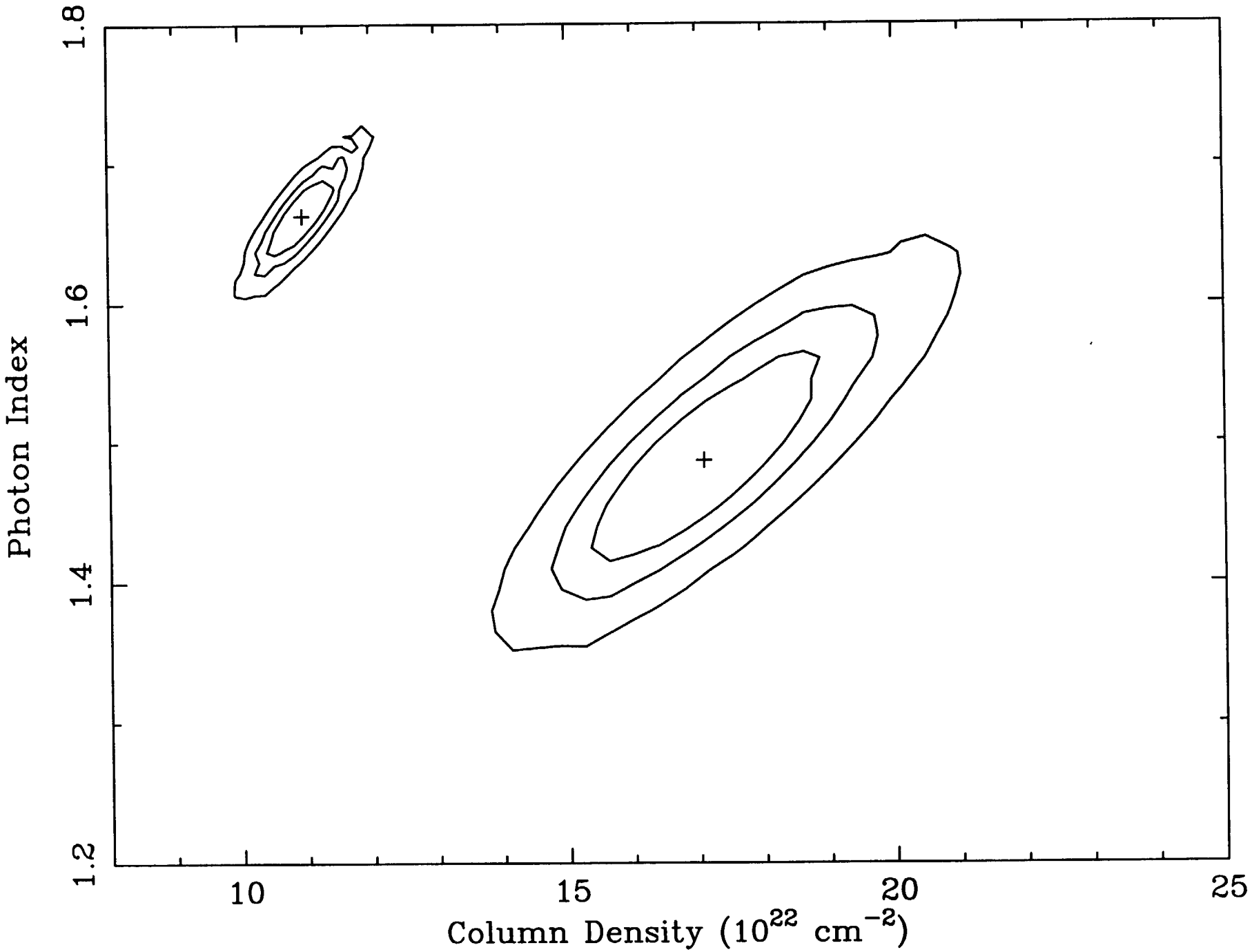
Photon Index
1.8
1.6
1.4
1.2
10
15
20
25
Column Density (10^{22} cm^{-2})